Implementation and validation of a new weather filter for reducing weather effect in the ASMR2 sea ice concentration data

Kohei Cho [1,*], Misako Kachi [2], Rigen Shimada [2], and Josefino Comiso [3]

[1] Tokai University, Tokyo, Japa; kohei.cho@tokai.ac.jp
[2] JAXA, Tsukuba, Japan; kachi.misako@jaxa.jp, shimada.rigen@jaxa.jp
[3] NASA, Maryland, United States; josefino_comiso@yahoo.com

Keywords: passive microwave radiometer；GCOM-W; bootstrap algorithm; atmospheric effect.

Abstract

Passive microwave radiometers observe the Earth's surface under practically all weather conditions, providing continuous global sea ice distributions on a daily basis. Ice concentration (IC) is one of the most important sea ice parameters derived from brightness temperatures measured by the microwave radiometers. However, even at microwave frequencies, the brightness temperature data over open ocean areas are affected by adverse weather conditions, including atmospheric water vapor, cloud liquid water, and abnormal water waves. The net result is the retrieval of moderate sea ice concentration values in the open ocean where sea ice is not expected. The current sea ice algorithms make use of what is called a “weather filter” to correct false sea ice retrievals, but significant areas in the ice-free water that have the false ice cover still remain. In this study, an improved weather filter, namely the Advanced Weather Filter (AWF), that minimizes this problem, developed by Cho et al. (2023), was implemented to produce JAXA/AMSR2 sea ice concentration products of the Arctic for verification. The AWF was validated and shown to be very effective in selected study regions in the Arctic during the summer from 30 June to 3 July 2014 and the winter from 15 December to 18 December 2014, thereby supporting the integration of the AWF into the standard AMSR2 sea ice concentration product. The AWF should be broadly applicable and can be implemented in other satellite passive microwave ice concentration datasets.

1. Introduction

1.1 Sea Ice Concentration

Long-term monitoring of sea ice with passive microwave radiometers onboard satellites, such as SSM/I on DMSP satellites, AMSR on ADEOS-2 satellite, AMSR-E on EOS/Aqua satellite and AMSR2 on GCOM-W satellite (JAXA, 2012), enabled the quantification of the variability and trend of global sea ice distribution (Parkinson et al., 1999, Comiso et al., 2008, IPCC, 2014). Because of relatively long wavelength that allows the retrieval of surface data under day/night, cloudy, and most weather conditions, passive microwave radiometers are powerful tools for monitoring the global distribution of sea ice continuously on a daily basis. Ice concentration (IC) is one of the most important sea ice parameters which can be calculated from brightness temperatures measured by passive microwave radiometers. There have been many algorithms developed to retrieve sea ice concentration, including the NASA Team Algorithm (Cavalieri et al., 1984), the Bootstrap Algorithm (Comiso, 1995), and the ASI Algorithm (Spreen et al., 2008). JAXA has adopted the AMSR2 Bootstrap Algorithm (Comiso, et al., 2013) as the standard algorithm for producing AMSR2 ice concentration dataset. Figure 1 shows the schematic diagram for calculating ice concentration (IC) in the AMSR2 Bootstrap Algorithm. In the scatter plot of 36GHz Vertical polarization (V) versus 18GHz Vertical polarization (V), open water (IC=0%) data are located near the point labeled O, while near consolidated ice (IC=100%) is distributed around the line PQ according to the emissivity and/or temperature differences of sea ice. For each AMSR2 data point, labeled as S as shown in the scatter plot, the ice concentration can be estimated by drawing a line from O through S to F, which is the point where the line intersects the consolidated ice line PQ, as shown in Figure 1. Since point O is regarded as 0% ice while point F corresponds to 100% ice, the ice concentration can be estimated by taking the ratio of the length of the line OS and that of OF as indicated in the following equation:

$$IC = m / l \quad (1)$$

Where m= length of line OS
l= length of line OF

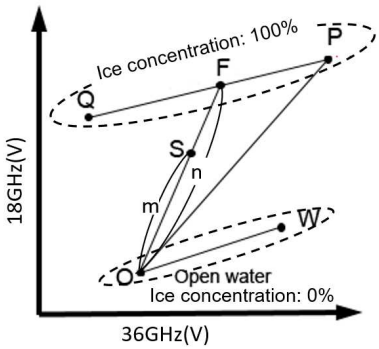

Figure 1. Schematic diagram of calculating ice concentration in the Bootstrap Algorithm.

Note that the location of point O is fixed in the algorithm and is expected to represent the brightness temperature of open water during relatively calm weather conditions and stable surface water, as can be found inside the ice pack. The signature of ice-free water can vary a lot, depending on weather and surface roughness conditions, and is usually represented by data points along the line OW. As a result, a weather filter is needed as described below.

1.2 False Sea Ice

Although microwaves can penetrate clouds, passive microwave radiation can be affected by various weather conditions, unusual atmospheric water vapor and cloud liquid water, and the roughening of the sea surface due to wind effects. This causes the brightness temperatures of some open water areas to be similar to those of sea ice covered areas. This issue has been referred to as “weather effects” (Gloersen et al., 1986). Such ice cover in the open ocean will be referred to as “false sea ice” in this paper. Figure 2 shows the AMSR2 IC images of the Bering Sea during a sequence of three days. A vast “sea ice area” (indicated by the red circle) is observed on the second day. It is unrealistic for sea ice to be missing on the first day, suddenly appear on the second day, and then disappear on the third day. Such sequences are a good indicator of the presence of “false sea ice”.

False sea ice has been observed in areas of the ocean where sea ice cover is not expected, in part because the sea surface is usually above freezing temperatures. Figure 3 shows the scatter plots of 36 GHz V vs 19 GHz V for open water, sea ice, and false sea ice around the data in the Bering Sea observed on 30 Dec. 2018. The gray dots represent sea ice, the blue dots are for open water, and the red dots are for false ice. Since the false sea ice data points overlap with those of sea ice-covered areas in the scatter plots, the algorithm retrieves some of the false sea ice areas as sea ice-covered areas.

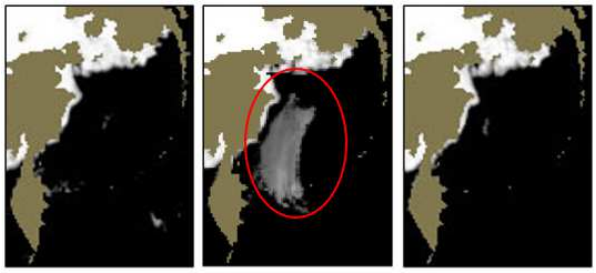

(1) 29 Dec. 2018 (2) 30 Dec. 2018 (3)31 Dec. 2018

Figure 2. Three-day sequential maps showing a vast false sea ice area observed on 30 December 2018 in the Bering Sea using AMSR2 IC images.

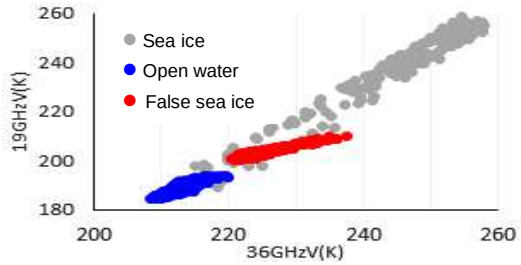

Figure 3. Scatter Plots of 19GHzV vs 36GHzV (Around the Bering Sea, 30 Dec. 2018

1.3 Progress of Weather Filter

To reduce the weather effects, a weather filter is usually incorporated in the sea ice concentration algorithms ((Comiso, 1995) and (Cavalieri et al., 1995)), but the technique has not been 100% effective, and the presence of residual false ice in the open ocean remains. Knowing the impact on ice variability and trend studies, historical daily data from SMMR, SSM/I, and AMSR-E data were inspected for residual false ice, and the latter was removed digitally / manually by setting the associated pixels to zero (or ice-free ocean). Such a process is quite laborious, and hence the desire to remove the false ice using an automated unsupervised system.

In recent years, due to the reduction of sea ice in the Arctic, the interest in Northern Sea Route linking Europe to Asia is increasing (JAMF, 2015), and the use of AMSR2 data for ship routing is considered (Sagawa, 2015). The large false sea ice in the sea ice concentration images derived from passive microwave sensors may reduce the reliability of those images. To improve the accuracy of sea ice concentration images and estimates of sea ice extent, enhancing the weather filter to reduce the presence of false ice is necessary.

Cho et al. started to investigate the ways to reduce the weather effect with AMSR-E data in 2010 (Cho et al., 2010), and improved the method step by step using AMSR2 data after the launch of AMSR2 onboard GCOM-W (Tezuka et al., 2013, Sugiura et al., 2016, Cho et al, 2015, 2020). However, the presence of residual false sea ice in some daily maps led to the current effort to further improve the technique, leading to the more effective weather filter described in the paper of Cho et al. (2023). In order to evaluate the legitimacy of implementing the filter for producing the AMSR2 sea ice standard product of JAXA, the filter was temporarily applied by JAXA to produce a limited number of the AMSR2 sea ice concentration products of the Northern Hemisphere for verification. This paper describes the verification result.

2. Test Sites and Analyzed Data

2.1 Test Sites

Since a large number of false sea ice areas appear in the Northern Hemisphere, the sea ice concentration images of the Northern Hemisphere were examined. Especially, the four areas in this hemisphere were examined in detail for the verification of the new weather filter: the Bering Sea, the Sea of Okhotsk, the Green Sea, and the Arctic coast of Russia. Figure 4 shows the location of the test sites. The Bering Sea is the northernmost part of the Pacific Ocean and is connected to the Arctic Ocean through the Bering Strait. The Sea of Okhotsk is located north of Japan, and the sea is one of the southernmost seasonal sea ice zones in the northern hemisphere. Accordingly, the false sea ice occasionally appears in both seas.

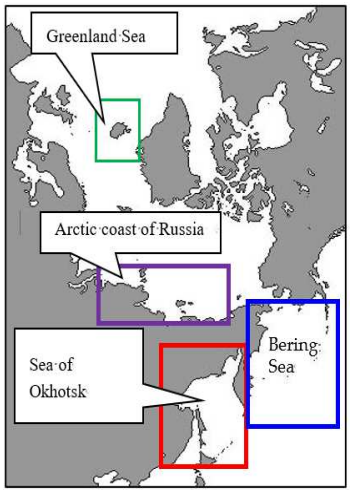

Figure 4. Test Sites

2.2 Analyzed Data

As for the data analysis, the brightness temperature data measured by the passive microwave radiometer AMSR2 and the sea ice concentration (IC) Level 3.0 data derived from the AMSR2 data using the AMSR2 Bootstrap Algorithm (Comiso et al., 2013) were used.

Table 1. Specifications of AMSR2 (JAXA, 2012)

frequency	resolution	polarization	swath width
7 GHz	35x62 km	Vertical/ Horizontal	1450km
10 GHz	24x42 km		
19 GHz	14x22 km		
23 GHz	15x26 km		
36 GHz	7x12 km		
89 GHz	3x5 km		

3. Methodology

3.1 Advanced Weather Filter

The following is a summary of our weather filter, developed for AMSR2 sea ice concentration calculations (Cho et al., 2023).
The basic idea of the weather filter is to set the sea ice concentration of the pixel to zero when the pixel value meets certain conditions. In the AMSR2 Bootstrap Algorithm, if the pixel value meets the following condition, the sea ice concentration of the pixel will be set to zero:

$$(TB23V\text{-}TB19V) > 19K \quad (2)$$

where TB23V and TB19V represent brightness temperatures of the vertical polarized (V) of 23GHz and 19GHz channels, respectively. This condition is based on the distribution of ice-free areas as illustrated in Figure 4 using the (TB23GHz-19GHz) vs TB36GHzV domain. The weather filter works well in many cases but not always. As a result, false sea ice occasionally appears in AMSR2 IC images as shown in Figure 2. By examining the brightness temperatures of false sea ice, the authors have changed the threshold level of equation (2) from 19K to 7K. The blue mesh area in Figure 5 indicates the additional pixels to be rejected as false sea ice. This can be done using equation (3) as given below.

$$(TB23V\text{-}TB19V) > 7K \quad (3)$$

In addition to equation (3), there is a need to impose the following two equations.

$$(TB36V\text{-}TB36H) > 57K \quad (4)$$

$$TB23V + 0.75 \times (TB36V - TB36H) < 250K \quad (5)$$

By applying these two equations, the false sea ice distributed in the pink colored area in the characteristic domain of (TB36V – TB36H) vs TB23V (see Figure 6) can be rejected. In the new weather filter, all the pixels that satisfy the equations (3), (4), and (5) are rejected as false sea ice. The authors have named the new weather filter as the Advanced Weather Filter (AWF).

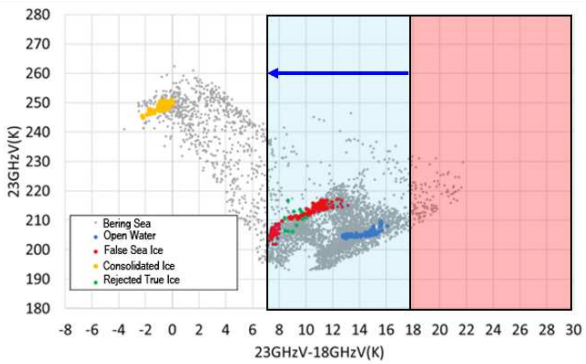

Figure 5. Weather filter threshold modification in the scatter plot of (TB23V-TB19V) vs (TB23V) .
(Bering Sea, Dec. 30, 2018)

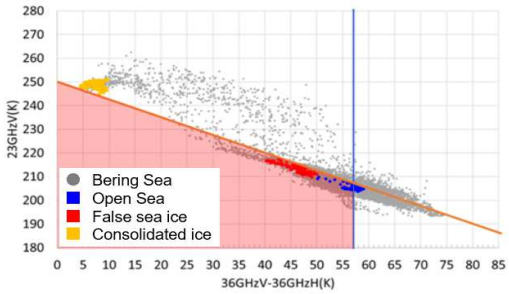

Figure 6. New Weather filter for rejecting the threshold setting in the scatter plot of (TB23V-TB19V) vs (TB23V)
(Bering Sea, Dec. 30, 2018)

3.2 Verification procedure

Although the initial development of AWF for AMSR2 made use of the 25 km ice concentration data, this study uses the 10 km data to be able to examine the effectiveness of the weather filter in greater spatial detail. The efficiency in rejecting false sea ice areas and the negative effect of rejecting true sea ice areas are both evaluated.

3.2.1 Selection of data

The authors have selected AMSR2 data for four consecutive days in winter, which include substantial false sea ice areas, and for four consecutive days in summer, which do not include apparent false sea ice areas. As for AMSR2 winter data, one-day composite images from 15 December to 18 December 2014 were selected. Apparent false sea ice areas are observed in the images of 15 and 17 December. As for ASMR2 summer data, one-day composite images from 30 June to 3 July 2014 were selected, which do not include any apparent false sea ice areas.

3.2.2 Efficiency of rejecting false sea ice areas

By observing as series of daily AMSR2 IC images of continuous days, vast sea ice areas that suddenly appear and disappear within one or two days were selected as false sea ice areas. After applying AWF to those AMSR2 IC images, the rejection performance of false sea ice areas was examined.

3.2.3 Identifying rejected true sea ice areas

The AWF is not perfect, and there are a few cases when areas that are actually covered by sea ice are rejected by the procedure and mistakenly labeled as false sea ice. In this study, the rejected sea ice areas other than the factual false sea ice areas are called “rejected true sea ice areas”. By calculating the histogram of the number of pixels for each ice concentration of “rejected true sea ice areas”, the negative effects of rejecting true sea ice areas were examined.

4. Verification Results

4.1 Winter (15 to 18 December 2014)

4.1.1 15 December 2014

Figure 7(a) shows the AMSR2 IC image of 15 December 2014. A vast false sea ice area is observed near Iceland, which disappears within one or two days during the ice growth period.

Figure 7(b) shows the ASMR2 IC image of the same day after applying AWF. Most of the false sea ice areas are well rejected by AWF. Figure 8(a) shows the rejected sea ice area in red color. Figure 8(b) is the zoomed-in image of the red rectangle area in Figure 8(a). In Figure 8(b), the rejected sea ice area is expressed as IC in rainbow color. The dark blue color dots in the purple box of Figure 8(b) show that the IC of the rejected pixels along the sea ice edge of the fast ice near Greenland are mostly less than the threshold level (15%) used for estimating sea ice extent. So, the rejection does not affect much the estimation of sea ice extent. To examine the total area of rejected true sea ice by AWF, the histogram of the whole sea ice areas, the rejected false sea ice area around Iceland, and the whole rejected sea ice area in the Northern Hemisphere were calculated. Figure 9(a) shows the histogram of total sea ice areas before AWF rejection. From Figure 9(a), we can see that most of the pixels in the image had ice concentrations over 90%. The maximum number of pixels for the IC was 54,064, corresponding to an IC value of 100%. Figure 9(b) shows the same histogram with the vertical axis scale set to 500 pixels to enhance the number of pixels for IC less than 80%. The total number of pixels for IC<80% was less than 300 pixels. The orange line in Figure 10 shows the histogram of the rejected sea ice area with AWF. The blue line shows the histogram of hole-rejected pixels, the red line shows the histogram of rejected false sea ice area around Iceland, and the green line shows the histogram of the rejected “real sea ice” along the sea ice edge as shown in the purple rectangle of Figure 8(b). The ice concentration of the rejected “real sea ice” pixels along the sea ice edge was less than 33%. Table 2 shows the statistics of rejected pixels with AWF. The total number of sea ice pixels within the images was 114,397. The total number of rejected pixels with AWF was 423, which corresponds to only 0.37% of the total sea ice pixels before applying AWF. If we confirm that only 300 of the rejected sea ice pixels around Iceland by AWF are false sea ice, the number of rejected “real sea ice” would be 123 pixels, which corresponds to only 0.11% of the total sea ice pixels before applying AWF. Statistically, this is almost negligible, and AWF may not affect the trend estimation of sea ice extent.

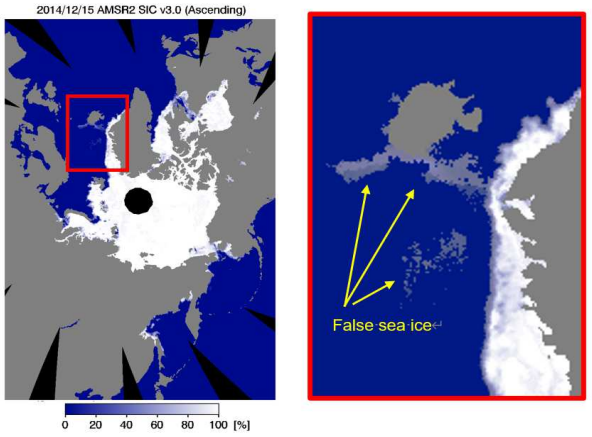

(a) Before AWF

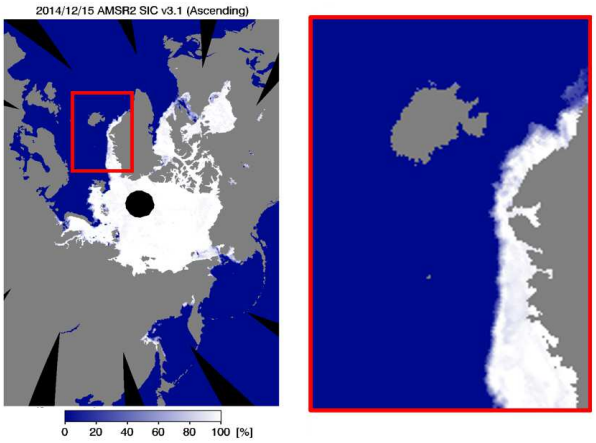

(b) After AWF

Figure 7. Ice concentration maps (a) before and (b) after AWF was applied to AMSR2 10 km data in the Arctic on 15 December 2014.

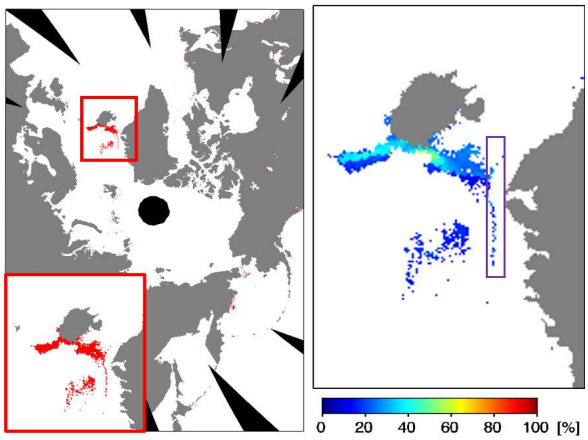

(a) Rejected area in red color (b)Rejected area in rainbow color

Figure 8. Extraction of the rejected sea ice area. (15 December 2014, Northern Hemisphere, IFOV:10km)

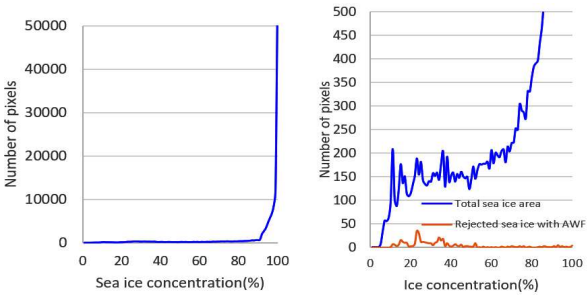

(a) Graph scaled for 50000 pixels (b) Graph scaled for 500 pixels

Figure 9. Histogram of the total sea ice area (in number of pixels) using10km AMSR2 data in the Northern Hemisphere on 15 December 2014.

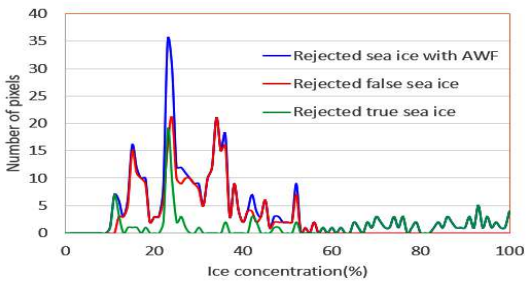

Figure 10. Histogram of total rejected pixels with AWF compared with those of actual false sea ice and rejected true sea ice using AMSR2 10 km IC data in the Northern Hemisphere on 15 December 2014.

Table 2. Statistics of rejected pixels with AWF

	Number of pixels	Percentage
Total number of sea ice pixels before applying AWF	114,397	100%
Total number of rejected pixels with AWF	423	0.37%
Total number of false sea ice around Iceland	300	0.26%
Total number of rejected “true sea ice”	123	0.11%

4.1.2 17 December 2014

Figure 11(a) shows the AMSR2 IC image of 17 December 2014. Huge false sea ice areas are observed near Greenland (green rectangle) and near Hokkaido, Japan (red rectangle), which disappeared within one day. The weather map in Figure 11(a) shows that a 948 hPa low-pressure system formed over the area (JMA, 2014). Figure 11(b) shows the ASMR2 IC image after applying AWF. Most of the false sea ice areas are well rejected by AWF. Some false sea ice remains near Greenland. However, if we change the parameters of AWF to reject all of the false sea ice, the number of rejected true sea ice will also be increased. This is the result of optimizing the parameters at this moment. Figure 12(a) shows the rejected sea ice area colored in red. Figure 12(b) is the zoomed-in image of the red rectangle area in Figure 12(a), which corresponds to the rejected “true sea ice” along the edge of fast sea ice abutting the coast of Greenland. The rejected “true sea ice” areas are shown in rainbow color in Figure 12(c) to enhance the ice concentration of each rejected pixel. It is clear that the ice concentrations of those rejected “true sea ice” areas are low.

Figure 13(a) shows the histogram of total sea ice areas before AWF rejection. From Figure 13(a), we can see that most of the pixels in the image had ice concentrations over 90%. The maximum number of pixels for the IC was 54,064, corresponding to an IC value of 100%. Figure 13(b) shows the same histogram with the vertical axis scale set to 500 pixels to enhance the number of pixels for IC less than 80%. The number of pixels for IC<80% was less than 324 pixels. The orange line in Figure 13(b) shows the histogram of the rejected sea ice areas with AWF. The orange line shows the histogram of rejected sea ice pixels, the red line shows the histogram of rejected false sea ice areas around Iceland, and the blue line shows the histogram of the rejected true sea ice areas. Table 3 shows the statistics of rejected pixels with AWF. The total number of sea ice pixels within the images was 116,726. The total number of rejected pixels with AWF was 2808, which corresponds to 2.41% of the total sea ice pixels before applying AWF. If we confirm that the rejected sea ice near Greenland (green rectangle in Figure 12(a)) and near Hokkaido (red rectangle in Figure 12(a)) are false sea ice, the number of rejected “true sea ice” would be 1124 pixels, which corresponds to only 0.96% of the total sea ice pixels before applying AWF. The statistics are summarized in Table 3.

4.1.3 16 & 18 December 2014

Figure 14 shows the AMSR2 IC images of 16 and 18 December 2014 with rejected sea ice area colored in red. No obvious false sea ice is observed in these images. The statistics of rejected sea ice areas are shown in Table 4. The total number of rejected pixels with AWF was less than 1% of the total sea ice areas in both images. Even if we assume that all the rejected pixels are true sea ice, the associated error when monitoring the trend of sea ice extent is relatively small.

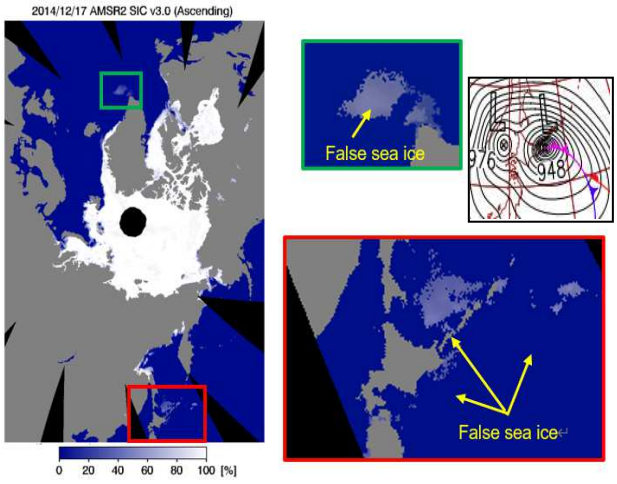

(a) Before AWF

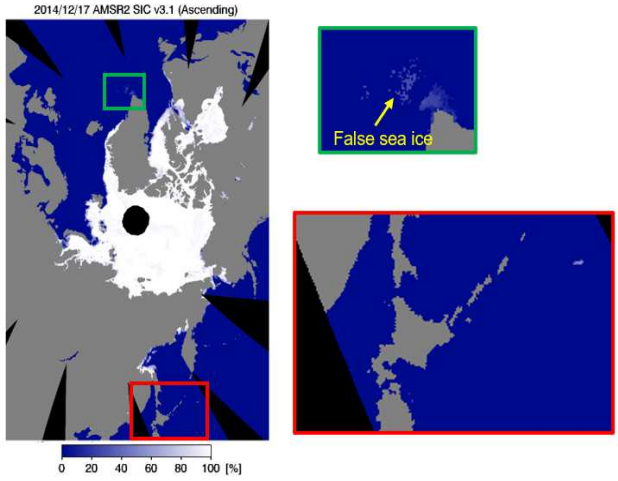

(b) After AWF

Figure 11. The effect of AWF applied to AMSR2 IC data (17 Dec. 2014, Northern Hemisphere, IFOV:10km)

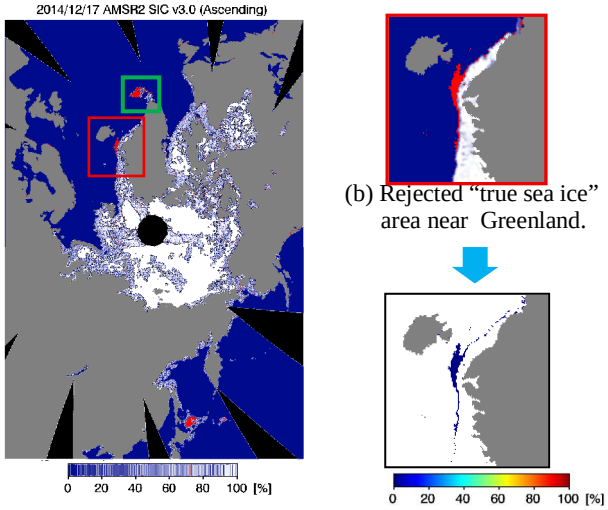

(a) Rejected area in red color

(b) Rejected “true sea ice” area near Greenland.

(c) Rejected “true sea ice“ area in rainbow color

Figure 12. Extraction of the rejected sea ice area. (17 Dec. 2014, Northern Hemisphere, IFOV:10km)

This contribution has been peer-reviewed. The double-blind peer-review was conducted on the basis of the full paper.
https://doi.org/10.5194/isprs-annals-XI-3-2026-655-2026 | © Author(s) 2026. CC BY 4.0 License.

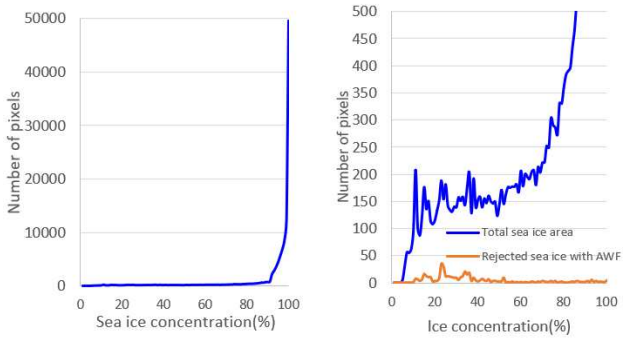

(a) Graph scaled for 50000 pixels (b) Graph scaled for 500 pixels

Figure 13. Histogram of the total sea ice area in number of pixels.
(17 Dec. 2014, Northern Hemisphere, IFOV:10km)

Table 3. Statistics of rejected pixels with AWF
(15 December 2014, Northern Hemisphere, IFOV:10km)

Items	Number of pixels	Percentage
Total number of sea ice pixels before applying AWF	116,726	100%
Total number of rejected pixels with AWF	2808	2.41%
Total number of rejected false sea ice	1684	1.44%
Total number of rejected “true sea ice”	1124	0.96%

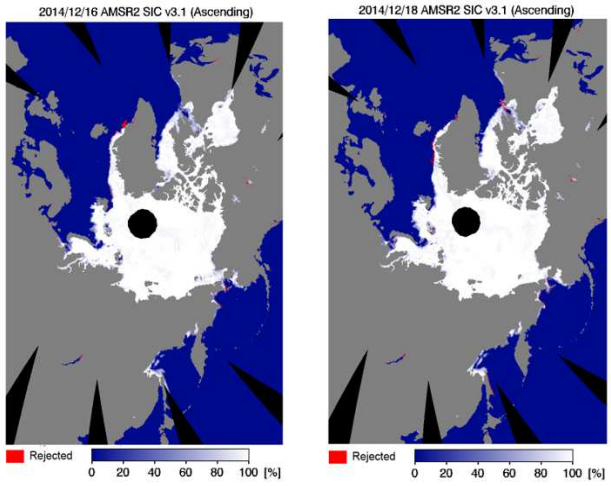

(a) 16 December 2014 (b) 18 December 2014

Figure 14. AMSR2 IC images with rejected areas colored in red (Northern Hemisphere, IFOV:10km)

Table 4. Statistics of rejected pixels with AWF
(1) 16 December 2014, Northern Hemisphere, IFOV:10km)

Items	Number of pixels	Percentage
Total number of sea ice pixels before applying AWF	114,331	100%
Total number of rejected pixels with AWF	407	0.36%

(2) 18 December 2014, Northern Hemisphere, IFOV:10km

Items	Number of pixels	Percentage
Total number of sea ice pixels before applying AWF	115,390	100%
Total number of rejected pixels with AWF	989	0.86%

4.2 Summer (30 June to 2 July 2014)

4.2.1 2 July 2014

Figure 15(a) shows the AMSR2 IC image of 2 July 2014 before applying AWF. No clear false sea ice is observed in this image. Figure 15(b) shows the ASMR2 IC image after applying AWF. The rejected sea ice area with AWF is enhanced in red. To examine in detail, the area along the coast of Russia in the Arctic was extracted as shown in Figure 16. The rejected sea ice could only be found at the ice edge and along the coastline. The total number of sea ice pixels within the images was 82,399. The total number of rejected pixels with AWF was 403, corresponding to only 0.49% of the total sea ice pixels before AWF. The total number of pixels rejected along the coast of Siberia was 57. Statistically, these are almost negligible. The histogram of the whole sea ice area, the rejected false sea ice area in the Arctic coast of Russia, and the whole rejected sea ice area were calculated and shown in Figure 17. From Figure 17(a), we can see that most of the pixels in the image had ice concentrations over 80%. The maximum number of pixels for the IC was 20,827, corresponding to an IC value of 100%. Figure 17(b) shows the same histogram with the vertical axis scale set to 500 pixels to enhance the number of pixels for IC less than 80%. The figure shows that the number of pixels for IC<80% is less than 500 pixels. The orange line in Figure 15(b) shows the histogram of the rejected sea ice area with AWF. Figure 16 shows the histogram of the rejected pixels with AWF. The orange line shows the histogram of rejected pixels, and the red line shows the histogram of rejected false sea ice area along the coast of Siberia. The ice concentration of the rejected sea ice along the sea ice edge was less than 54%.

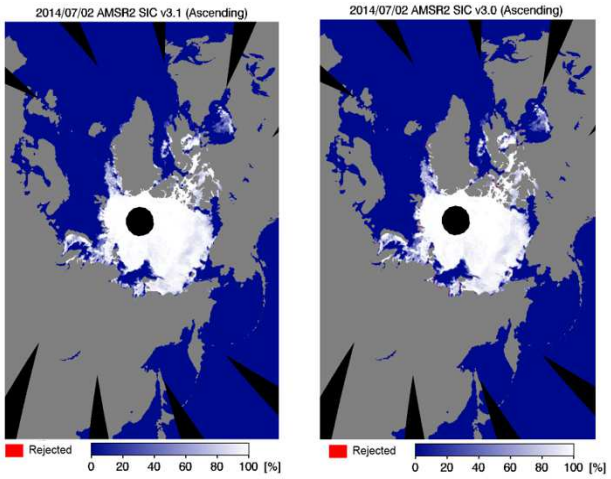

(a) Before AWF (b) After AWF

Figure 15. AMSR2 IC image of before and after applying AWF
(2 July 2014, Northern Hemisphere, IFOV:10km)

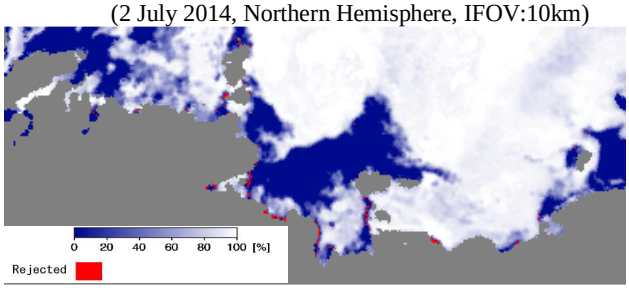

Figure 16. Extraction of the rejected sea ice areas.
(2 July 2014, Arctic coast of Russia, IFOV:10km)

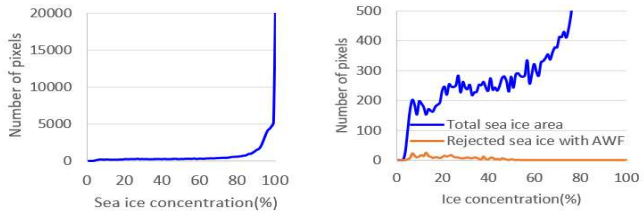

(a) Graph scaled for 50000 pixels (b) Graph scaled for 500 pixels

Figure 17. Histogram of the total sea ice area
(2 July 2014, Northern Hemisphere, IFOV:10km)

4.2.2 Total summary from 30 June to 2 July 2014

Table 5 shows the statistics of rejected pixels with AWF from 30 June to 2 July 2014.

Table 5. Statistics of rejected pixels with AWF

Date	Number of rejected pixels / Number of sea ice pixels	Percentage
30 June 2014	481 / 84,158	0.57%
1 July 2014	539 / 83,173	0.65%
2 July 2014	403 / 82,399	0.49%
3 July 2014	364 / 81,307	0.45%

5. Conclusion

Cho et al (2020) validated that the sea ice concentration data derived from AMSR2 using the Bootstrap Algorithm is quite reliable. However, a shortcoming of current algorithms for estimating sea ice concentration and extent is the retrieval of sea ice in the open ocean (referred to as “false sea ice” in this study), where sea ice is not expected. This effect does not happen so often. However, the presence of false ice in the data causes significant problems in the study of the spatial and temporal variability of the sea ice cover. Moreover, the presence of false sea ice in ice concentration images would provide incorrect information, especially for those involved in ship navigation and other activities in the polar regions.

In this study, the improved weather filter, namely the Advanced Weather Filter (AWF), developed by the authors primarily for GCOM-W/AMSR2 was applied to produce the AMSR2 sea ice concentration data for verification. The AWF was validated in the Northern Hemisphere using the AMSR2 10km sea ice concentration product in Summer, from 27 June to 3 July, and in Winter, from 15 to 18 December 2014. The detailed analysis in the study areas indicated that most of the false sea ice areas were identified by AWF (with ice concentration values reduced to zero). The rejection of false sea ice with AWF improves the accuracy of ice concentration maps and prevents overestimation of sea ice extent and sea ice area. Fortuitously, the percentage of true sea ice areas rejected in each image was 0.45-1.44% of the total sea ice area, which is statistically small and may not have a significant impact on estimates of trends and changes in global sea ice extent. However, considering the high variability in weather/surface conditions, more case studies are needed to better assess the uncertainties associated with AWF.

Following this result, JAXA decided to apply AWF for producing the standard product of AMSR2 sea ice concentration for the Northern Hemisphere. It will also be used to process data from AMSR3, launched on 24 June 2025. The technique can also be used for any passive microwave radiometer data that has the required frequency and polarization channels.

Acknowledgement

This study was performed under the sponsorship of the JAXA 3rd Research Announcement on the Earth Observation (EO-RA3). The authors would like to thank Ms. Mieko Seki of RESTEC for technically supporting our study. The authors also acknowledge the valuable contributions of Dr. Kazuhiro Naoki and past students of Cho Lab. at Tokai University to the development of AWF.

Abbreviations: The following abbreviations are used in this manuscript:
SSM/I: Special System Microwave Imager
DMSP: Defense Meteorological Satellite Program
AMSR: Advanced Microwave Scanning Radiometer
ADEOS: Advanced Earth Observing Satellite
GCOM-W: Global Change Observation Mission-Water
IPCC: Intergovernmental Panel on Climate Change
SMMR: Scanning Multichannel Microwave Radiometer
NASA: National Aeronautics and Space Administration
JAXA: Japan Aerospace and Exploration Agency

References

Cavalieri, D. J. and Gloersen, P., 1984, “Determination of sea ice parameters with the NIMBUS 7 SMMR”, J. Geophys. Res., Vol.89, pp.5355-5369.

Cavalieri, D. J., Germain, K. M. St., and Swift, C. T., 1995, Reduction of weather effects in the calculation of sea ice concentration with the DMSP SSM/I. Journal of Glaciology. (41, 139) 455-464.

Cho, K., Nishiura, K., 2010, A study on cloud effect reduction for extracting sea ice area from passive microwave sensor data, The International Archives of the Photogrammetry, Remote Sensing and Spatial Information Sciences, Vol. XXXVIII-Part 8, pp.1042-1045.

Cho, K., Naoki, K., 2015, Advantages of AMSR2 for Monitoring Sea Ice from Space, Proceedings of the 36th Asian Conference on Remote Sensing, WE4.8, pp.1-8.

Cho, K., Naoki, K., and Comiso, J. C., 2020, Detailed validation of AMSR2 sea ice concentration data using MODIS data in the Sea of Okhotsk, ISPRS Ann. Photogramm. Remote Sens. Spatial Inf. Sci., V-3-2020, 369–373, https://doi.org/10.5194/isprs-annals-V-3-2020-369-2020.

Cho, K., Naoki, K. 2023, A New Weather Filter For Reducing Weather Effect in Calculating Sea Ice Concentration from AMSR2 Data, ISPRS Ann. Photogramm. Remote Sens. Spatial Inf. Sci., X-1-W1-2023, 793–798, https://doi.org/10.5194/isprs-annals-X-1-W1-2023-793-2023.

Comiso, J. C., 1995, SSM/I Sea Ice Concentrations Using the Bootstrap Algorithm, NASA Reference Publication 1380, Maryland, NASA Center for AeroSpace Information, Available online:http://www.geobotany.uaf.edu/library/pubs/ComisoJC1995_nasa_1380_53.pdf.

Comiso, J. C. and Nishio, F., 2008, Trends in the sea ice cover using enhanced and compatible AMSR-E & SMMR, J. Geophys. Res., Vol. 113, C02S07, pp.1-22.

Comiso, J. C. and Cho, K., 2013, Description of GCOM-W1 AMSR2 Sea Ice Concentration Algorithm, Descriptions of GCOM-W1 AMSR2 Level 1R and Level 2 Algorithms, JAXA, NDX-120015A, (6)1-28, Available online:http:// suzaku.eorc.jaxa.jp/ GCOM_W/data/doc/NDX-120015A.pdf

Gloersen, P. and Cavalieri, D. J., 1986, Reduction of weather effects in the calculation of sea ice concentration from microwave radiances, J. Geophys. Res., (l.91)3913-3919.

IPCC, 2014, “Summary for Policymakers.” In Climate Change 2013: The Physical Basis. Contribution of Working Group I to the Fifth Assessment Report of the Intergovernmental Panel on Climate Change, edited by Stocker, T.F., Qin, D., Plattner, G.K., *et al*. Cambridge: Cambridge University Press.

Japan Association of Marine Safety (JAMF), 2015, https://www.nikkaibo.or.jp/pdf/NorthernSeaRouteHandbook_E.pdf

JAXA, 2012, https://suzaku.eorc.jaxa.jp/GCOM_W/ w_amsr2 /amsr2_body_main.html.

JMA, 2014, weather maps, https://www.data.jma.go.jp/yoho/ data/hibiten/2014/201412.pdf

Parkinson, C. L., Cavalieri, D. J., Gloersen, P., Zwally, H. J., and Comiso, J. C., 1999, Arctic sea ice extents, areas, and trends, 1978– 1996, J. Geophys. Res., Vol.104, C9, 20837–20856.

Sagawa, G., 2015, Satellite Watch Over the Northern Sea Route, https://global.jaxa.jp/article/2015/special/satellite/sagawa.html

Spreen, G., Kaleschke, L., and Heygster, G., 2008, Sea ice remote sensing using AMSR-E 89 GHz channels, J. Geophys. Res., vol. 113, C02S03, doi:10.1029/2005JC003384.

Sugiura. S., Naoki, K., Cho, K., 2016, Atmospheric Effect Reduction in Calculating Sea Ice Concentration From AMSR2 Data, Proceedings of the 37th Asian Conference on Remote Sensing, Ab0569, pp.1-4.

Tezuka, T., Cho, K., 2013, Reduction of Atmospheric Effects in Sea Ice Concentration Estimation Using Satellite Microwave Radiometer AMSR2, Proceedings of the 34th Asian Conference on Remote Sensing, SC01, pp.332-338.